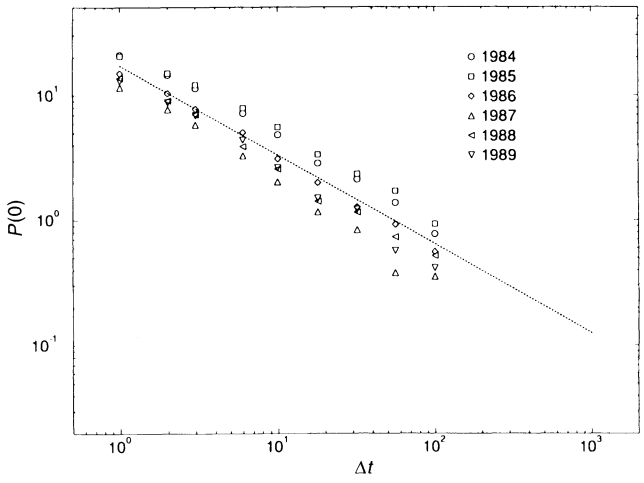

FIG. 3 Probability of return $P(0)$ of the S&P 500 index variations as a function of the time sampling intervals observed in different years. The same scaling behaviour of the complete set of data (dotted line) is observed each year (data are parallel to the dotted line). The scale factor γ is slowly time-dependent, as the vertical positions of the probability of return change from year to year.

1.38 ± 0.14) and γ fluctuates more than α, having bursts of activity localized in specific months (such as April 1987, and October 1987 and immediately following months).

We compare our experimental results with the statistical properties of the heteroskedastic stochastic process GARCH(1, 1) (ref. 18). We simulate GARCH(1, 1) processes characterized by control parameters close to the values obtained in the time-series analysis of stock returns[22]. We find that the time evolution of the probability density functions (PDFs) of the GARCH(1, 1) process is quite different from that observed in the experimental data. In particular, we investigate the probability of return to the origin of the GARCH(1, 1) simulated process using the values of the control parameters selected to mimic the experimental $\Delta t =$ 1 min PDF, and find the data are fitted well by a straight line in a log–log plot, with slope -0.531 ± 0.025. The scaling index is therefore 1.88 ± 0.09, a value close to 2 but 43% larger than the value of 1.4 observed in the experimental data. □

Received 12 September 1994; accepted 1 June 1995.

1. Bak, B., Tang, C. & Wiesenfeld, K. *Phys. Rev. Lett.* **59,** 381–384 (1987).
2. Nelkin, M. *Adv. Phys.* **43,** 143–181 (1994).
3. Meneveau, C. & Sreenivasan, K. R. *J. Fluid. Mech.* **224,** 429–484 (1991).
4. Olami, Z., Feder, H. J. S. & Christensen, K. *Phys. Rev. Lett.* **68,** 1244–1247 (1992).
5. Peng, C.-K. *et al. Phys. Rev. Lett.* **70,** 1343–1346 (1993).
6. Brock, W. A. in *The Economy as a Complex Evolving System* (ed. Anderson, P. W., Arrow, J. K. & Pines, D.) 77–97 (Addison-Wesley, Redwood City, 1988).
7. Brock, W. A., Hsieh, D. A. & LeBaron, B. *Nonlinear Dynamics, Chaos, and Instability: Statistical Theory and Economic Inference* (MIT Press, Cambridge, MA, 1991).
8. Scheinkman, J. A. & LeBaron, B. *J. Business* **62,** 311–327 (1989).
9. Shlesinger, M. F., Frisch, U. & Zaslavsky, G. (eds) *Lévy Flights and Related Phenomena in Physics* (Springer, Berlin, 1995).
10. Bouchaud, J.-P. & Georges, A. *Phys. Rep.* **195,** 127–293 (1990).
11. Shlesinger, M. F., Zaslavsky, G. M. & Klafter, J. *Nature* **363,** 31–37 (1993).
12. Bachelier, L. J. B. *Théorie de la Speculation* (Gauthier-Villars, Paris, 1900).
13. Osborne, M. F. M. *Oper. Res.* **7,** 145–173 (1959).
14. Mandelbrot, B. B. *J. Business* **36,** 394–419 (1963).
15. Fama, E. F. *J. Business* **38,** 34–105 (1965).
16. Clark, P. K. *Econometrica* **41,** 135–155 (1973).
17. Engle, R. F. *Econometrica* **50,** 987–1007 (1982).
18. Bollerslev, T., Chou, R. Y. & Kroner, K. F. *J. Econometrics* **52,** 5–59 (1992).
19. Officer, R. R. *J. Am. statist. Ass.* **67,** 807–812 (1972).
20. Hsu, D.-A., Miller, R. B. & Wichern, D. W. *J. Am. statist. Ass.* **69,** 108–113 (1974).
21. Lau, A. H.-L., Lau, H.-S. & Wingender, J. R. *J. Business Econ. Statist.* **8,** 217–223 (1990).
22. Akgiray, V. *J. Business* **62,** 55–80 (1989).
23. Mantegna, R. N. *Physica* **A179,** 232–242 (1991).
24. Tucker, A. L. *J. Business Econ. Statist.* **10,** 73–81 (1992).
25. Lévy, P. *Théorie de l'Addition des Variables Aléatoires* (Gauthier-Villars, Paris, 1937).
26. Brock, W. A. & Kleidon, A. W. *J. Econ. Dyn. Contr.* **16,** 451–489 (1990).
27. Mantegna, R. N. & Stanley, H. E. *Phys. Rev. Lett.* **73,** 2946–2949 (1994).
28. Shlesinger, M. F. *Phys. Rev. Lett.* **74,** 4959 (1995).
29. Feller, W. *An Introduction to Probability Theory and Its Applications* (Wiley, New York, 1971).
30. Akgiray, V. & Booth, G. G. *J. Business Econ. Statist.* **6,** 51–57 (1988).

ACKNOWLEDGEMENTS. We thank S. V. Buldyrev and K. Simons for important contributions in the early stages of this work, and J. Gonzalo, M. A. Salinger and S. Zapperi for helpful discussions. This work was supported by the US NSF.

Dynamics of formation of symmetrical patterns by chemotactic bacteria

Elena O. Budrene* & Howard C. Berg*†

* Department of Molecular and Cellular Biology, Harvard University, 16 Divinity Avenue, Cambridge, Massachusetts 02138, USA
† Rowland Institute for Science, 100 Edwin H. Land Boulevard, Cambridge, Massachusetts 02142, USA

MOTILE cells of *Escherichia coli* aggregate to form stable patterns of remarkable regularity when grown from a single point on certain substrates. Central to this self-organization is chemotaxis, the motion of bacteria along gradients of a chemical attractant that the cells themselves excrete[1]. Here we show how these complex patterns develop. The long-range spatial order arises from interactions between two multicellular aggregate structures: a 'swarm ring' that expands radially, and focal aggregates that have lower mobility. Patterning occurs through alternating domination by these two sources of excreted attractant (which we identify here as aspartate). The pattern geometries vary in a systematic way, depending on how long an aggregate remains active; this depends, in turn, on the initial concentration of substrate (here, succinate).

Under certain conditions, cells of chemotactic strains of *Escherichia coli* and *Salmonella typhimurium* excrete an attractant, aggregate in response to gradients of that attractant, and form patterns of varying cell density[1–3]. This process occurs only if cells are chemotactic towards aspartate, and can be suppressed by addition of aspartate or aspartate analogues. In *E. coli*, aggregates form in the wake of a travelling circular band, producing highly symmetrical patterns[1]. Their geometry depends on initial conditions; for example, the concentration of growth substrate. In *S. typhimurium*, aggregates arise from the centre of an unstructured bacterial lawn, producing patterns with lower symmetry[2]. The present work was undertaken to determine the mechanism by which *E. coli* forms patterns with long-range spatial order and why particular geometries arise at different initial concentrations of substrate. Succinate and fumarate both work well[1]; we used succinate.

Patterns appear within a certain range of succinate concentrations (Fig. 1). The concentrations of growth substrate required for each pattern vary from strain to strain, but for a given strain, the succession of patterns observed with increasing concentrations is fixed. At low concentrations of succinate, one sees a single compact travelling band (swarm ring) that moves slowly outwards (Fig. 1*a*). At higher concentrations, spots appear in concentric rings in radial rows (that is, on a pseudo-rectangular lattice), Fig. 1*b*, then in sets of intersecting spirals (that is, on a pseudo-hexagonal lattice), Fig. 1*c*, and finally on a pseudo-hexagonal lattice but with radial tails, Fig. 1*d*. As evident in Fig. 1*d* and documented below, the spots form in the wake of a band of cells moving outwards at the periphery of the pattern. An unstructured zone of low cell density always precedes the first element of a pattern. The radius of this zone decreases with increasing concentration of substrate. The radial periods and circumferential spacings differ from strain to strain, from about 1 to 6 mm. At even higher concentrations of substrate, one obtains more elaborate patterns, with radial streaks, indented rings, or petals (not shown). These patterns are not as reproducible, even in replicate plates, and some geometries appear only with certain strains.

To understand how changes in one initial condition, the concentration of succinate, can so dramatically alter the pattern-forming behaviour of the system, we studied effects of succinate concentration on bacterial growth and chemotaxis. The growth rate of *E. coli* in succinate saturates and is approximately constant over the concentration range 0.5–7 mM, in agreement with

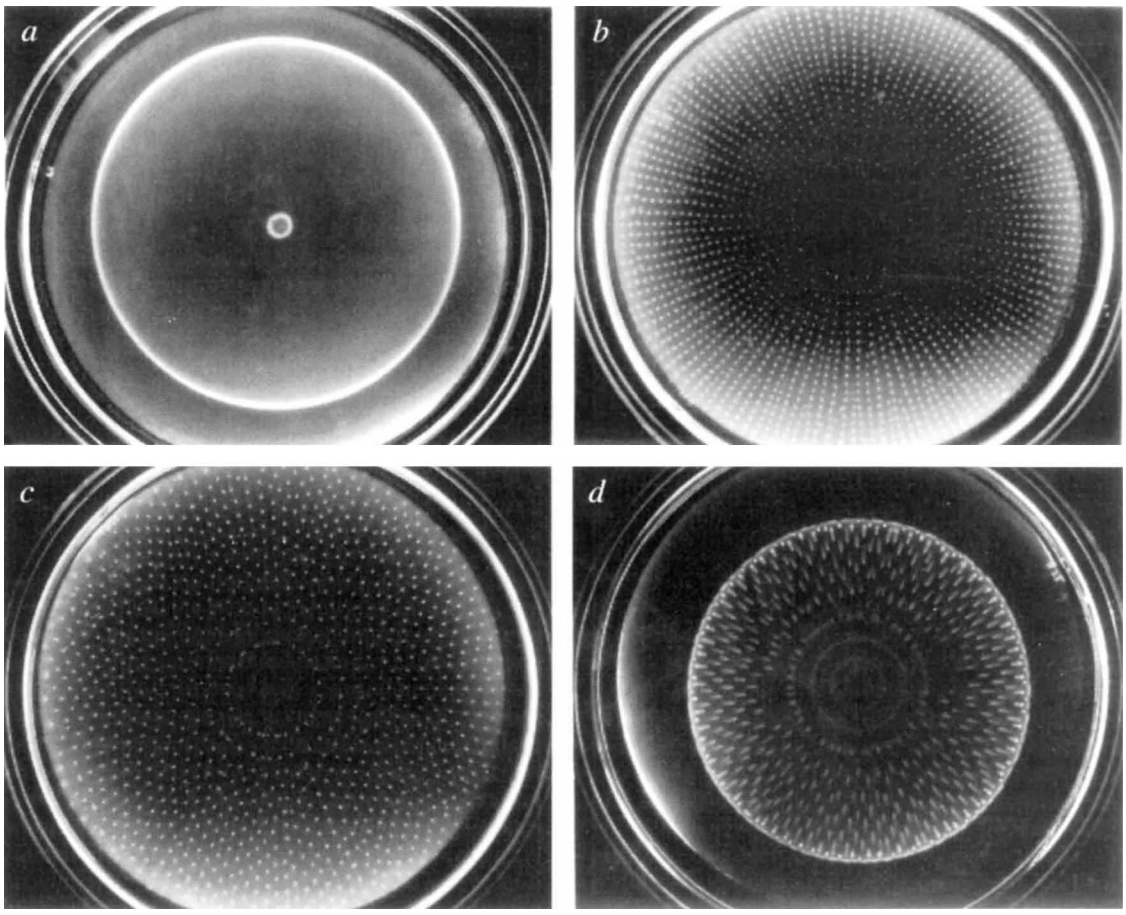

FIG. 1 Patterns generated by cells of *E. coli* chemotactic towards aspartate. With increasing concentrations of substrate (here, succinate) one obtains a swarm ring or a swarm ring followed by spots on a rectangular lattice, spots on a hexagonal lattice, or spots with tails on a hexagonal lattice (see ref. 1, Fig. 1*b*, *a*, *d*, respectively). *a*, A swarm ring generated by *E. coli* strain HCB317 (deleted for *tsr*, the gene that specifies the serine receptor[14]) grown on 1 mM succinate. An aspartate-blind mutant (not shown) generates, instead, an expanding disk of much lower, uniform cell density. *b*, Spots on a pseudo-rectangular lattice, generated by the same strain grown on 2 mM succinate. *c*, Spots on a pseudo-hexagonal lattice generated by the same strain grown on 3 mM succinate. *d*, Spots with tails on a pseudo-hexagonal lattice generated by cells of strain RP4368 (a serine-blind point mutant; from J. S. Parkinson) grown on 3 mM succinate. A similar pattern can be generated with strain HCB317 (not shown).

METHODS. Growth was in plastic Petri plates (8.5 cm internal diameter) containing 10 ml of medium. Stock solutions of ingredients for M9 minimal medium[15] plus substrate and amino-acid supplements (L forms of threonine, leucine, histidine and methionine, 20 μg ml^{-1} of each) were combined on each plate with 0.24% water agar (Difco Laboratories, Detroit). The vital dye tetrazolium red or tetrazolium violet (50 μg ml^{-1}, Sigma) was added to improve image contrast. The plates were allowed to harden at room temperature on a level table for 2 h. Then they were inoculated at the centre with 5 μl of fresh saturated culture, pregrown in M9-glycerol (33 mM) and incubated in a level humid chamber at 25 °C. They were photographed 38, 72, 72 and 48 h later, respectively, from above on Polaroid 667 film against a dark background, illuminated slantwise from below by two circular fluorescent lamps.

the classic Monod relation[4]. Under our conditions (see Fig. 1 legend) the doubling time is ~2 h. On the other hand, the final cell density is roughly proportional to the initial concentration of succinate (Fig. 2*a*). The rate of excretion of the attractant aspartate also increases with the concentration of succinate (Fig. 2*b*). Finally, the rate of expansion of the swarm ring decreases with the concentration of succinate (Fig. 4*c*). With strain HCB317, the swarm ring forms after ~24 h, then advances at a constant rate. If the concentration of succinate is greater than 1.3 mM, aggregates appear at ~32 h.

The swarm ring of Fig. 1*a* is not the same as the chemotactic ring that appears when cells consume a metabolizable attractant[5,6]. In order for the ring of Fig. 1*a* to form, cells must excrete an attractant. This attractant is aspartate. Neither swarm rings nor patterns form in soft agar with an *aspA* mutant under any set of conditions. This mutant (*E. coli* strain C58 Asp 28, ref. 7) is motile and chemotactic but fails to excrete aspartate (E.O.B. and H.C.B., unpublished results). The defect is in aspartase (L-aspartate ammonia-lyase, EC 4.3.1.1), an enzyme that aminates fumarate.

It is likely that migration of the swarm ring requires an asymmetric aspartate profile, with a higher concentration of aspartate at the leading edge of the ring than at its trailing edge. This would be expected if the cells consume a substantial fraction of the succinate, thus decreasing the rate of excretion of aspartate at the trailing edge (Fig. 2*b*). Because the cells grow at a constant rate, this takes longer at higher succinate concentrations, explaining why the rate of expansion of the swarm ring is smaller at higher concentrations (Fig. 2*c*). An alternative possibility for the generation of an asymmetric aspartate profile is that cells at the trailing edge of the swarm ring are starved of ammonia, and so metabolize aspartate at a greater rate[2,8].

Time-lapse video recordings were made at higher magnification to reveal events that take place in the vicinity of the swarm ring (Fig. 3). Generation of the pseudo-rectangular lattice begins when the swarm ring breaks into discrete spots (Fig. 3*a*, 0 h). A spot forms at one point along the circumference, and then new spots appear in succession on each side, so that the ring fragments both clockwise and anticlockwise at the rate of about 5 cm h^{-1} (not shown). The first set of aggregates is left behind, while the swarm ring continues on its way (2.5 h). Later, the aggregates disintegrate, and many of their cells stream forward to rejoin the swarm ring (3.8 h). A subset remains to mark the spot where a given aggregate first formed. Finally, new aggre-

gates form at the points where cells rejoined the swarm ring (5.9 h). Then the process recycles: compare 5.9 with 0 h, 7.2 with 2.5 h, and 8.5 with 3.8 h. A third set of aggregates appears at 9.5 h, and a fourth at 13.4 h. Thus, one obtains radial arrays of spots on concentric circles. At a large radius, when the circumferential spacing exceeds a certain threshold, an intervening aggregate appears, and a new radial row is initiated (Fig. 1*b*).

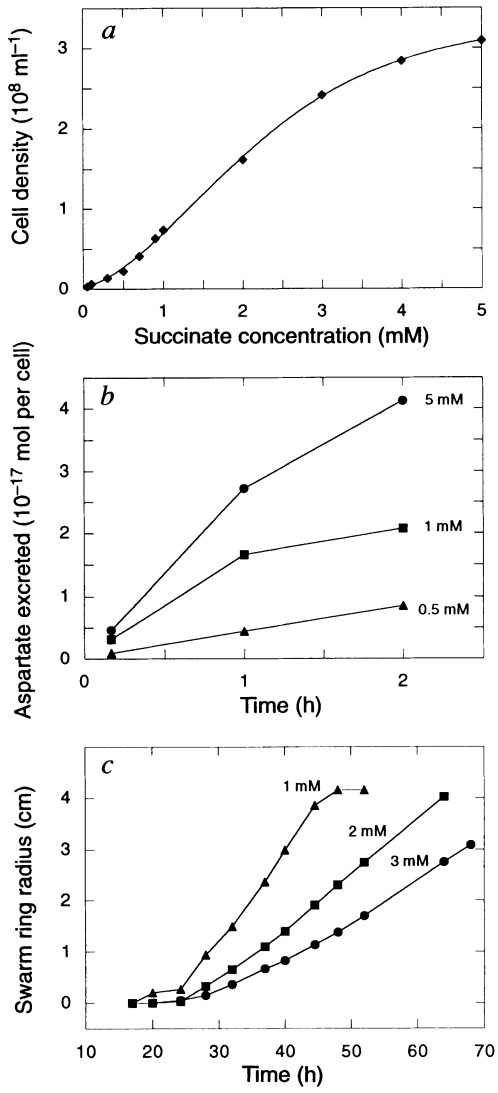

FIG. 2 Processes affected by substrate concentration. *a*, Final cell density; *b*, rate of excretion of aspartate; and *c*, radius of swarm rings, plotted as a function of time.

METHODS. All experiments were done with strain HCB317 (Fig. 1*a*) at 25 °C. *a*, Bacteria at low titre were inoculated in 10-ml aliquots of liquid medium (without agar) in Petri plates and incubated without shaking in the humid chamber. Final concentrations were determined from the absorbance at 600 nm, using the conversion factor for our spectrophotometer of 8×10^8 cells per absorbance unit. Replicate plates gave essentially identical results. *b*, Cells were pregrown on M9-succinate (5 mM) to mid-exponential phase (1.4×10^8 cells per ml), then washed and incubated in 5 mM ammonium acetate (pH 7.0) supplemented with succinate at concentrations of 0.5, 1 and 5 mM at densities of 2.2, 2.0 and 2.5×10^8 cells per ml, respectively. Aliquots were removed at different times, the cells were filtered out, the supernatant fraction was freeze-dried, and its aspartate content was determined in an amino-acid analyser (using pre-derivatization with phenylisothiocyanate, Applied Biosystems 420ABI). *c*, Agar plates with 1, 2 or 3 mM succinate (five at each concentration) were inoculated with 5 μl of cells pregrown on M9-succinate (5 mM) to mid-exponential phase and diluted to 1.2×10^7 cells per ml in M9 buffer. The diameter of the swarm ring was measured approximately every 3 h with a ruler. Mean radii are shown, limited to ~4 cm by the size of the plate; the standard deviations were smaller than the symbols on the plots.

With the pseudo-hexagonal lattice (Fig. 3*b*) there are two sets of aggregates forming and disintegrating at any one time, roughly half a cycle out of phase. Cells streaming toward the swarm ring from disintegrating aggregates in one row pass between aggregates that have just formed in the next row (0.6, 1.8 h). As before, new aggregates form where cells from earlier aggregates join the swarm ring. But now these aggregates tend to act independently: they move forward with the swarm ring, then stop and disintegrate. This independent behaviour is even more striking at higher substrate concentrations, when radial tails appear (Fig. 3*c*). Now, the nucleus of an aggregate moves as an intact structure, leaving cells in its wake that form a streak with diminishing width. The length of this streak (the radial tail) reflects the distance covered by the decaying aggregate.

When discrete aggregates first form, their cells are highly motile; after they disintegrate, the cells left behind are not. Therefore, stabilization of a pattern is achieved through loss of motility. Cells left behind in disintegrated aggregates were removed from plates and resuspended in motility medium[9]. Most were non-motile or failed to respond to aspartate. Some of these cells produced motile progeny after growth on hard agar, but others did not. Thus, the transition to the non-motile state is due to changes in both phenotype[10] and genotype.

How, then, are the patterns formed? The cells grow on succinate and excrete aspartate. A chemotactic response to aspartate, which is distributed asymmetrically as the cells grow, amplifies spatial inhomogeneity. A swarm ring forms at the periphery of the growing colony, and then the cells advance as a group away from the point of inoculation. Given time for cells to proliferate, the cell density within the swarm ring increases, and fluctuations in the local concentration of aspartate become large enough to trigger the formation of a discrete aggregate. Because the cell doubling time is constant whereas the rate of expansion of the swarm ring decreases with increasing substrate concentration (Fig. 2*c*), the first aggregate appears at a smaller radius at higher substrate concentrations (Fig. 1). Formation of this aggregate destabilizes the swarm ring. Other cells in the swarm ring move towards this aggregate, depleting regions to either side, generating a gradient of aspartate that is positive near the aggregate but negative farther away. Thus, more distant cells move away from the first aggregate, increasing the density farther away, where two new aggregates appear. This process continues in both directions around the ring until a complete set of aggregates has formed. Cells that are not recruited into this set remain in the swarm ring and continue on their way. Eventually, the density of the swarm ring increases to the point where new aggregates form. Naively, one would expect these aggregates to appear in between the earlier ones, as more cells remain in those regions after the first set has formed (for example, Fig. 3*a*, 7.2 h). Indeed, this is the way in which the hexagonal lattice is initiated (see below). However, at low concentrations of succinate, the original set of aggregates begins to run out of succinate and to excrete less aspartate. The gradient generated by the advancing swarm ring becomes dominant, and cells that remain chemotactic in the original set of aggregates stream forward to rejoin the swarm ring (for example, Fig. 3*a*, 8.5 h), leaving defective cells behind. This influx rapidly carries the local cell density over the aggregation threshold, and a new set of aggregates forms that are radially in-line with the first (for example, Fig. 3*a*, 9.5 h). The cells left behind are non-motile, and the pattern is frozen in.

At higher concentrations of succinate, cells remain in the aggregated state longer than they do at lower concentrations, mainly because it takes longer to use up the available succinate. Studies of time-lapse recordings made at the earliest stages of the development of hexagonal patterns show that the second set of aggregates tends to form in the swarm ring in between the first set; that is, the cell density there reaches threshold before the old aggregates begin to disintegrate (not shown). Once this

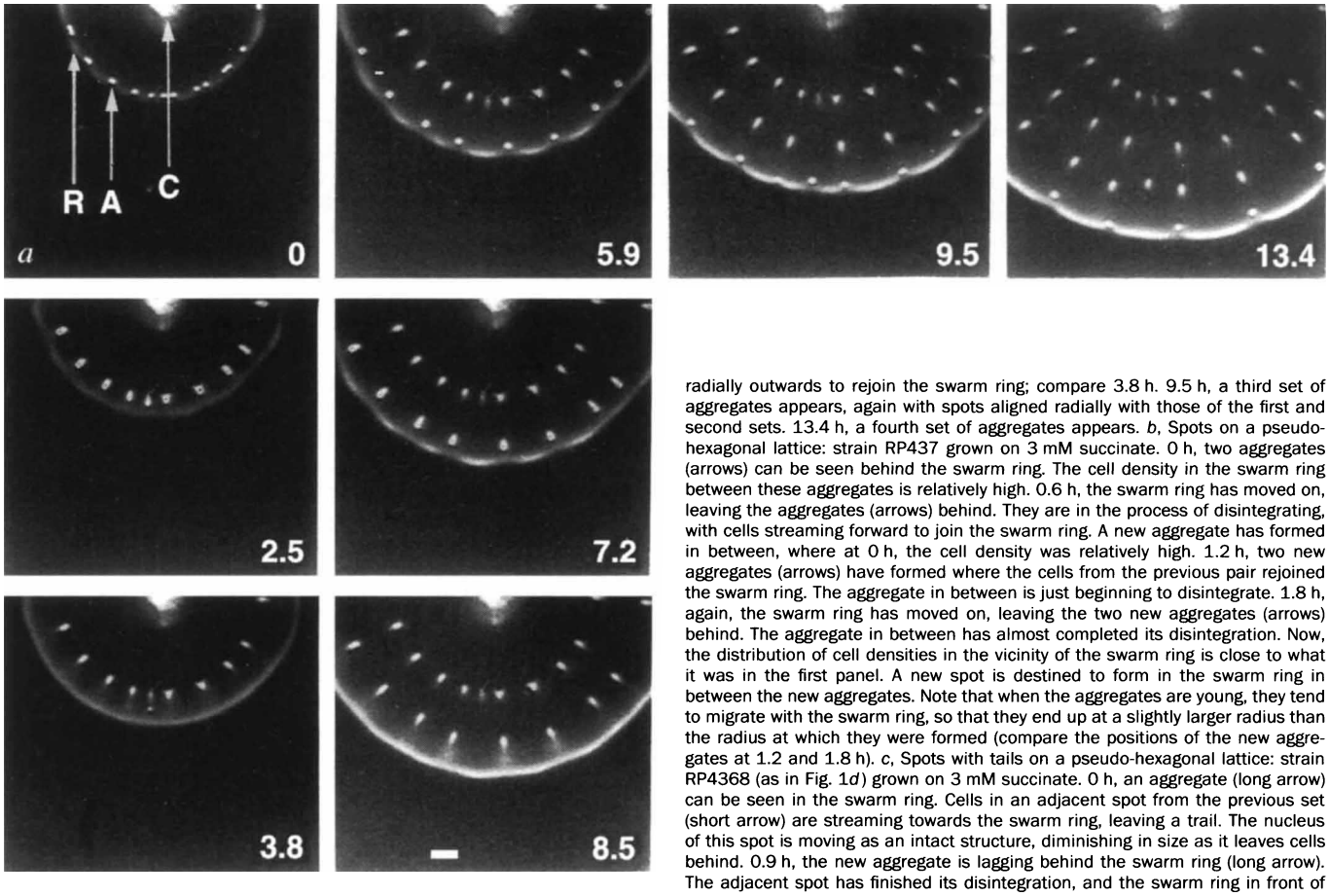

FIG. 3 Microscopic behaviour resulting in patterns of the kind shown in Fig. 1. The panels in each set of prints are labelled by elapsed time in h since the first panel. Scale bar, 2 mm. *a*, Spots on a pseudo-rectangular lattice: *E. coli* strain RP437 (wild-type for chemotaxis[16]) grown on 2 mM succinate. This pattern was recorded near the centre of the plate (C), where the spots are more widely dispersed. 0 h, an expanding swarm ring (R) breaking into aggregates (A). Note the stretches of swarm ring remaining between aggregates. 2.5 h, the swarm ring moves radially outwards, leaving the aggregates behind. The cell density in the swarm ring is higher between aggregates. 3.8 h, the aggregates disintegrate, and many of their cells stream radially outwards to rejoin the swarm ring. 5.9 h, a second set of aggregates appears in the swarm ring, with spots forming at the points of arrival of the cells from the first set. 7.2 h, once again, the swarm ring moves radially outwards, leaving the aggregates behind; compare with 2.5 h. 8.5 h, the second set of aggregates disintegrates, and many of their cells stream radially outwards to rejoin the swarm ring; compare 3.8 h. 9.5 h, a third set of aggregates appears, again with spots aligned radially with those of the first and second sets. 13.4 h, a fourth set of aggregates appears. *b*, Spots on a pseudo-hexagonal lattice: strain RP437 grown on 3 mM succinate. 0 h, two aggregates (arrows) can be seen behind the swarm ring. The cell density in the swarm ring between these aggregates is relatively high. 0.6 h, the swarm ring has moved on, leaving the aggregates (arrows) behind. They are in the process of disintegrating, with cells streaming forward to join the swarm ring. A new aggregate has formed in between, where at 0 h, the cell density was relatively high. 1.2 h, two new aggregates (arrows) have formed where the cells from the previous pair rejoined the swarm ring. The aggregate in between is just beginning to disintegrate. 1.8 h, again, the swarm ring has moved on, leaving the two new aggregates (arrows) behind. The aggregate in between has almost completed its disintegration. Now, the distribution of cell densities in the vicinity of the swarm ring is close to what it was in the first panel. A new spot is destined to form in the swarm ring in between the new aggregates. Note that when the aggregates are young, they tend to migrate with the swarm ring, so that they end up at a slightly larger radius than the radius at which they were formed (compare the positions of the new aggregates at 1.2 and 1.8 h). *c*, Spots with tails on a pseudo-hexagonal lattice: strain RP4368 (as in Fig. 1*d*) grown on 3 mM succinate. 0 h, an aggregate (long arrow) can be seen in the swarm ring. Cells in an adjacent spot from the previous set (short arrow) are streaming towards the swarm ring, leaving a trail. The nucleus of this spot is moving as an intact structure, diminishing in size as it leaves cells behind. 0.9 h, the new aggregate is lagging behind the swarm ring (long arrow). The adjacent spot has finished its disintegration, and the swarm ring in front of it is more dense (short arrow). 2.1 h, the new aggregate is in the process of disintegration, its nucleus moving as a unit toward the swarm ring, leaving a trail (long arrow). Another aggregate has formed in the swarm ring at the point where cells from the adjacent spot joined it (short arrow). 4.1 h, the disintegration of the aggregate formed at 0 h is now nearly complete. The adjacent aggregate is beginning to disintegrate.

METHODS. As in Fig. 1, but recorded with a CCD camera (Hamamatsu XC-77 with C2400 control, with different extension tubes and a 50-mm lens) and a time-lapse video recorder (JVC BR-9000U, triggered manually by a homemade pulse generator). The fluorescent lamps were run continuously and cooled with a fan, and a sheet of heat-absorbing glass was placed below the Petri plate. The inside of the lid of the Petri plate was coated with a detergent (Triton X-100, Sigma) to prevent accumulation of droplets of condensed water. Selected frames were output on a video printer (Sony UP-870MD).

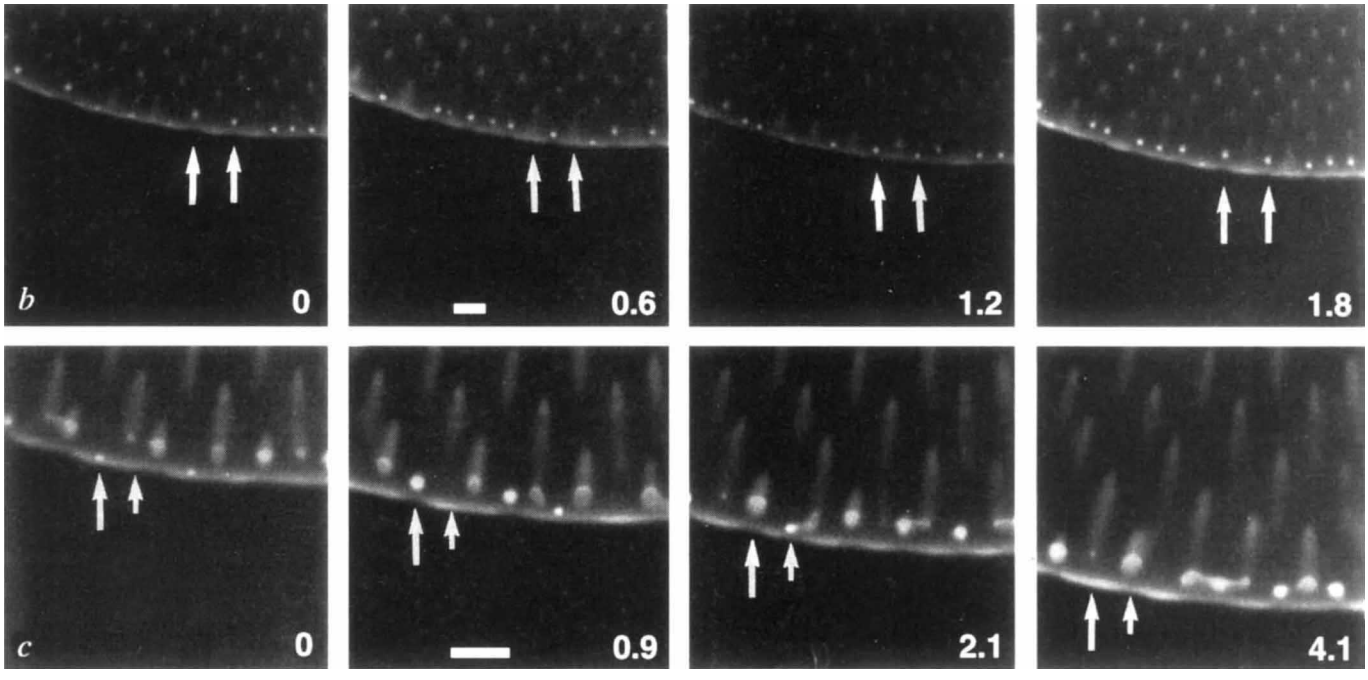

happens, a cycle is established in which adjacent aggregates in successive rows are born, mature and disintegrate in an alternating sequence (Fig. 3*b*). Finally, at even higher concentrations of succinate, local excretion of aspartate is sufficient to keep the centre of an aggregate intact, even when its cells are responding *en masse* to an external gradient. Less-responsive cells that fall behind generate tails which, like those of a comet, point outwards from the centre. Were this trend to continue, one would expect to find aggregates with long lifetimes that move about like multicellular organisms. *E. coli* does, in fact, form such structures (that we call 'slugs') and these orchestrate the development of the more elaborate patterns mentioned earlier (E.O.B. and H.C.B., manuscript in preparation).

In brief, excretion of aspartate by *E. coli* allows cells to form two well-defined multicellular structures, an advancing swarm ring and focal aggregates. Interactions between these structures determine the positions of emerging elements in the developing pattern. Models for pattern formation proposed thus far do not embody this mechanism. A continuous model by Bruno[11] assumes constant production of a stable attractant, and produces isolated spots without higher-order correlations. Continuous and discrete models by Ben-Jacob *et al.*[12] produce higher-order correlations, but with mechanisms requiring either autocatalytic production of attractant triggered by levels of toxic waste, or by addition of a second (repellent) chemotactic signal. We do not believe that either mechanism is required. In our view, variations in the rate of excretion of attractant determined by cell density and the availability of substrate will suffice. In any event, the chemotactic behaviour of the swarm ring and the focal aggregate should be modelled in detail; several questions need to be answered. How is the identity of the swarm ring maintained, and what determines its rate of migration? What dictates the separation of bacteria between swarm ring and aggregate? Under what conditions can an aggregate move as an intact structure, and what sets its life expectancy?

Formation of spatial patterns from a mass of initially identical cells is one of the central problems of developmental biology. Rapid progress has been made in understanding the genetic control of morphogenesis (see ref. 13 for a review). However, genetics does not always reveal the dynamics of interactions involved. As seen here, a simple system involving motile responses to a diffusible substance can have surprising consequences. Substrate consumption, cell proliferation, excretion of attractant, and chemotactic motility, when combined in a certain way, can generate complex spatial structures; a specialized morphogenetic program is not required. With bacteria, these processes can be modulated independently in a controlled manner, allowing accurate tests of quantitative models for pattern formation. □

Received 31 March; accepted 31 May 1995.

1. Budrene, E. O. & Berg, H. C. *Nature* **349,** 630–633 (1991).
2. Woodward, D. E. *et al. Biophys. J.* **68,** 2181–2189 (1995).
3. Blat, Y. & Eisenbach, M. *J. Bact.* **177,** 1683–1691 (1995).
4. Neidhardt, F. C., Ingraham, J. L. & Schaechter, M. *Physiology of the Bacterial Cell* 208 (Sinauer Associates, Sunderland, MA, 1990).
5. Adler, J. *Science* **153,** 708–716 (1966).
6. Nossal, R. *Expl Cell. Res.* **75,** 183–142 (1972).
7. Marcus, M. & Halpern, Y. S. *Biochim. biophys. Acta* **177,** 314–320 (1969).
8. Gutnick, D., Calvo, J. M., Klopotowski, T. & Ames, B. N. *J. Bact.* **100,** 215–219 (1969).
9. Adler, J. & Templeton, B. *J. gen. Microbiol.* **46,** 175–184 (1967).
10. Parkinson, J. S. *Genetics* **116,** 499–500 (1987).
11. Bruno, W. J. *CNLS Newsletter* Vol. 82, 1–10 (Centre for Nonlinear Studies, Los Alamos National Lab., Los Alamos, 1992).
12. Ben-Jacob, E. *et al. Nature* **373,** 566–567 (1995).
13. Barinaga, M. *et al. Science* **266,** 561–614 (1994).
14. Wolfe, A. J., Conley, M. P., Kramer, T. J. & Berg, H. C. *J. Bact.* **169,** 1878–1885 (1987).
15. Miller, J. H. *Experiments in Molecular Genetics* 431 (Cold Spring Harbor Lab., New York, 1972).
16. Parkinson, J. S. *J. Bact.* **135,** 45–53 (1978).

ACKNOWLEDGEMENTS. This paper is dedicated to Julius Adler on the occasion of his sixty-fifth year. We thank B. J. Bachman for the *aspA* strain, L. Turner for help with Fig. 2, M. A. Nilsson for photographic work, and M. Meister and J. A. Shapiro for comments on the manuscript. This work was supported by the US NSF and the Rowland Institute for Science.

Terminal Proterozoic reorganization of biogeochemical cycles

Graham A. Logan*, J. M. Hayes*, Glenn B. Hieshima*† & Roger E. Summons‡

* Biogeochemical Laboratories, Departments of Geological Sciences and of Chemistry, Indiana University, Bloomington, Indiana 47405-1403, USA
‡ Australian Geological Survey Organisation, PO Box 378, Canberra, ACT 2601, Australia

THE Proterozoic aeon (2,500–540 million years ago) saw episodic increases in atmospheric oxygen content[1], the evolution of multicellular life[2,3] and, at its close, an enormous radiation of animal diversity[3]. These profound biological and environmental changes must have been linked, but the underlying mechanisms have been obscure. Here we show that hydrocarbons extracted from Proterozoic sediments in several locations worldwide are derived mainly from bacteria or other heterotrophs rather than from photosynthetic organisms. Biodegradation of algal products in sedimenting matter was therefore unusually complete, indicating that organic material was extensively reworked as it sank slowly through the water column. We propose that a significant proportion of this reworking will have been mediated by sulphate-reducing bacteria, forming sulphide. The production of sulphide and consumption of oxygen near the ocean surface will have inhibited transport of O_2 to the deep ocean. We find that preservation of algal-lipid skeletons improves at the beginning of the Cambrian, reflecting the increase in transport by rapidly sinking faecal pellets. We suggest that this rapid removal of organic matter will have increased oxygenation of surface waters, leading to a descent of the O_2–sulphide interface to the sea floor and to marked changes in the marine environment, ultimately contributing to the Cambrian radiation.

Hydrocarbons extractable from sedimentary rocks of Proterozoic age are often enriched in ^{13}C relative to the associated insoluble organic debris[4–6]. When this same relationship, which reverses that found between extractable lipids and total biomass in living organisms, is observed in more recent strata, it usually indicates that the soluble compounds have migrated from some other source. That this is not the case for the Proterozoic sediments is confirmed by our present analyses of organic materials from well preserved Proterozoic units. As shown in Fig. 1*a*, *n*-heptadecane is enriched in ^{13}C relative to kerogen (for which δ values vary due to secular trends that have been widely recognized as characteristic of Proterozoic strata[7,8]), but pristane, a probable product of the degradation of chlorophyll and thus related to primary inputs, is isotopically depleted. No known source of contamination or migrating fluids would provide this combination of enrichment and depletion.

The depletion of ^{13}C in lipids relative to total biomass is characteristic of all autotrophs and respiring heterotrophs. The reversed relationship shown in Fig. 1*a* cannot, therefore, indicate simply that Proterozoic organisms used different biosynthetic pathways and thus fractionated isotopes differently. Instead, an ecological factor, something related to the processing of organic material after biosynthesis but before burial, must be responsible. In Phanerozoic and modern systems, isotopic enrichment is associated with heterotrophic reworking[9,10]. It does not generally produce geolipids enriched in ^{13}C relative to coexisting kerogen, but could if effects were strongly accentuated and made appropriately selective at the molecular level.

Pathways of carbon flow during most of the Proterozoic differed from those in later times because organic matter pro-

† Present address: Exxon Production Research Company, PO Box 2189, Houston, Texas 77252-2189, USA.